RSC Advances

PAPER

Cite this: *RSC Adv.*, 2015, **5**, 98955

# Liponitroxides: EPR study and their efficacy as antioxidants in lipid membranes†

Giovanna Mobbili,[a] Emanuela Crucianelli,[a] Antonio Barbon,[c] Massimo Marcaccio,[d] Michela Pisani,[b] Annalisa Dalzini,[c] Eleonora Ussano,[d] Marco Bortolus,*[ce] Pierluigi Stipa*[b] and Paola Astolfi*[b]

Received 15th September 2015
Accepted 3rd November 2015

DOI: 10.1039/c5ra18963b

www.rsc.org/advances

A series of lipid-functionalized nitroxides having a pyrroline nitroxide moiety linked either to a glycerol or to a steroid unit has been synthesized, and their inclusion inside phospholipid bilayers has been investigated by Electron Paramagnetic Resonance (EPR) spectroscopy. The antioxidant behavior of these nitroxides has been studied in azo-initiator induced lipid peroxidation by means of the Thiobarbituric Acid Reactive Species (TBARS) assay; a correlation with their penetration depth within the bilayer has been found. The possible mechanisms involved in the antioxidant action have been considered, discussed and alternative pathways have been suggested for the synthesized liponitroxides due to their different localization. The steroid derivative is limited to scavenging radicals that are generated in the aqueous phase, while the glycerolipids can also act as chain breaking antioxidants.

## Introduction

Lipid peroxidation (LP) is a critical and common damaging process in biological membranes and liposomial dispersion containing polyunsaturated fatty acids (PUFAs). The associated damage is highly detrimental to the functioning of the cell and its survival, since membranes form the basis of many cellular organelles like mitochondria, plasma membranes, lysosomes, peroxisomes, *etc.* Thus, prevention of LP represents an interesting therapy in many diseases and pathologies involving free radicals[1] and is also an important aspect in the preparation and preservation of liposomes to be used as carriers for several agents in medicinal, pharmaceutical, cosmetic and food industry applications.

In this context cyclic nitroxides (aminoxyls), stable compounds with an unpaired electron on the N–O function included in an aliphatic or aromatic ring system, have gained popularity as a distinct class of antioxidants thanks to their protective effects against oxidative stress in a multiplicity of biological systems.[2] It has been shown that nitroxides effectively protect cells, tissues, organs, and animals from radical-induced damage and that these antioxidant activities derive from their abilities to scavenge radicals,[3] catalyze superoxide dismutation,[4] facilitate catalase-like activity of heme-proteins,[5] detoxify hypervalent metals, and oxidize reduced transition metals ions.[6] The antioxidant activity of both aliphatic[7] and aromatic[8] nitroxides against radical-induced LP has been extensively studied due to the importance and seriousness of this phenomenon. In fact, their reactivity toward lipid derived radicals ($L^{\bullet}$) *via* radical–radical coupling is well known and documented, whereas more controversial is that toward oxygen-centred radicals (ROS, reactive oxygen species)[9] which is still debated.[10] However, it has been shown that nitroxides are able to reduce alkylperoxyl radicals forming the corresponding oxoammonium cations ($>N^{+}{=}O$) and that a relationship between the oxidation potentials of nitroxides and their peroxyl radicals scavenging abilities exists.[10a] Since peroxyl radicals are important intermediates in LP, it follows that the antioxidant power of a nitroxide against lipid peroxidation should be determined by its radical scavenging ability as well as its redox potential. However, these are not the only aspects that demand consideration, given the complexity of biological lipid membranes and of LP, a process in which the formation of the damaging species is not uniform across the membrane. Since the peroxidation normally takes places at the fatty acids double bonds, which are located at specific positions in the bilayers, the structure of the nitroxide, its penetration as well as its

[a]*Department of Life and Environmental Sciences, Università Politecnica delle Marche, Via Brecce Bianche 12, I-60131 Ancona, Italy*

[b]*Department of Materials, Environmental Sciences and Urban Planning, Università Politecnica delle Marche, Via Brecce Bianche 12, I-60131 Ancona, Italy. E-mail: p.stipa@univpm.it; p.astolfi@univpm.it*

[c]*Department of Chemical Sciences, Università di Padova, Via Marzolo 1, I-35131 Padova, Italy. E-mail: marco.bortolus@unipd.it*

[d]*Department of Chemistry "G. Ciamician", Università di Bologna, Via Selmi 2, I-40126 Bologna, Italy*

[e]*Department of Material Sciences, Università degli Studi di Milano Bicocca, Via Roberto Cozzi 55, I-20125 Milano, Italy*

† Electronic supplementary information (ESI) available: Spectroscopic characterization of liponitroxides. Cyclic voltammetric curves of **Chol-NO** at low temperature in THF; background cyclic voltammetric curves for 0.08 M $NaBF_4$ aqueous electrolyte solution with PBS buffer at pH = 7.4. Accessibility parameters $\Pi_i$ to oxygen and to NiEDDA. See DOI: 10.1039/c5ra18963b

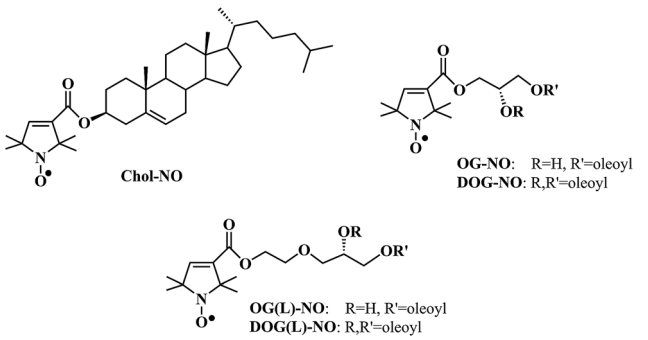


Chart 1 Lipid-functionalized nitroxides **NOXs** synthesized and tested for their antioxidant activity.

Table 1 Half-wave ($E_{1/2}$) redox potentials (*vs.* NHE) of studied species at 298 K

| Species[a] | (Red) – $E_{1/2}$/V | (Ox) – $E_{1/2}$/V |
|---|---|---|
| **DOG-NO**[a] | −1.58[b,c] | 1.33 |
| **OG(L)-NO**[a] | −1.57[b,c] | 1.31 |
| **OG(L)-NO**(ads) | — | 1.12 |
| **Chol-NO**[a] | −1.59[b,c] | 1.32 |
| **Chol-NO**(ads)[d] | −1.07[c] | 1.16 |

[a] In a 0.08 M $TBAPF_6$/THF solution. [b] Sluggish electrochemical process. [c] Irreversible process, peak potential. [d] Drop casted species on GC electrode in a 0.08 M $NaBF_4$ aqueous solution buffered (pH = 7.4) with phosphate buffer.

mobility in the membrane interior have also to be taken into account. For these reasons, lipid-functionalized nitroxides that have a good affinity for lipid bilayer are attractive molecules to be used as antioxidants, but so far, they have been synthesized mainly as potential spin probes for Electron Paramagnetic Resonance (EPR) spectroscopy[11] in the context of membrane structure studies.[12] Only in one case the antioxidant activity of two steroidic nitroxyl radicals has been also studied.[7a]

In this work, a series of lipid-functionalized nitroxides (**NOXs**) has been synthesized (Chart 1) with the double aim of locating the nitroxide at different depths inside the lipid membrane, and to look for relationships between their location and antioxidant activity. These compounds have a pyrroline nitroxide linked to a cholesterol unit or to glycerol esterified with one or two oleoyl moieties. In particular, the glycerol-functionalized nitroxides contain one (**OG-NO**/**OG(L)-NO**) or two (**DOG-NO**/**DOG(L)-NO**) oleic acid chains, which may differently anchor the molecule into the lipid bilayer. Moreover, two of the **NOXs** have a polar spacer group in the headgroup region (**OG(L)-NO** and **DOG(L)-NO**), which is expected to push the pyrroline nitroxide toward the lipid–water interface. The electrochemical behaviour of the synthesized compounds has been studied both in THF solution and in an aqueous environment to evaluate their oxidation potential. The position, orientation and dynamics of the **NOXs** inside the bilayer have been determined using different EPR techniques both in liposomes (small unilamellar vesicles, SUV) and in bicelles.[13] Finally, the antioxidant activity of the synthesized **NOXs** has been studied during radical-induced peroxidation of egg-yolk L-α-phosphatidylcholine (Egg-PC) liposomes, chosen as model membranes, and discussed on the basis of their position inside the lipid.

# Results

### Redox properties

The electrochemical investigation of the nitroxide species was carried out by cyclic voltammetry (CV) in tetrahydrofuran (THF) and in solid state as film in aqueous electrolyte solution (drop-casting the nitroxide lipid onto glassy carbon (GC) disk electrode surface) in aqueous electrolyte solution, at room temperature, using platinum and GC disk as working electrode. THF was chosen as it has a relatively low dielectric constant and so the species are in an environment more similar to that inside a bilayer. The redox potentials of three among the synthesized compounds are collected in Table 1 which are representative for all the others. In fact, it is reasonable to admit that the structure of the lipid portion of the molecule does not substantially affect the redox activity centred on the nitroxide unit.

The cyclic voltammetric curves of **Chol-NO**, in THF and in buffered aqueous solution (drop casted film onto a CG disk electrode) are reported in Fig. 1 (see also Fig. S1† for the electrochemical behaviour at 213 K and Fig. S2† for the background curves in aqueous electrolyte, in the ESI†). In both cases, it is possible to observe a reversible one-electron oxidation process with a half-wave potential of 1.32 V (THF) and 1.16 V (PBS) *vs.* NHE. This can be safely attributed[14] to the oxidation of the nitroxide moiety to form the oxoammonium cation $\rangle N{=}O^+$. On the negative potential side, a one-electron chemically irreversible reduction process can be observed with a cathodic peak potential of −1.59 V (THF) and −1.06 V (PB) *vs.* NHE.

As expected, no substantial differences were found between the redox potentials of the various **NOXs** since the portion of the molecule involved in the redox processes (the pyrroline moiety) is the same in all cases.

### Penetration depth

The dimensionless immersion depth parameter $\Phi$ was obtained by measuring the enhancement of the relaxation properties (which are related to the saturation of the EPR transitions) for the different **NOXs** generated by the collision of the radicals with paramagnetic relaxing agents having a different distribution inside and outside the membrane. By using either a lipophilic or a hydrophilic agent, respectively oxygen or the complex nickel-ethylenediamine-*N*,*N*′-diacetic acid (NiEDDA),[15] the relaxation properties of **NOXs** will be affected differently, depending on the localization of the nitroxide with respect to the plane of the phosphate groups of the bilayer. The position of the nitroxide relative to such a plane was obtained by comparing the results on the **NOXs** with those of nitroxide-labeled phospholipids (**SLs**)[15] used as standards: 1-palmitoyl-2-stearoyl-(*n*-doxyl)-sn-glycero-3-phosphocholine (*n*DPC) and 1-palmitoyl-2-oleoyl-sn-glycero-3-phospho(tempo)choline (TempoPC).

 

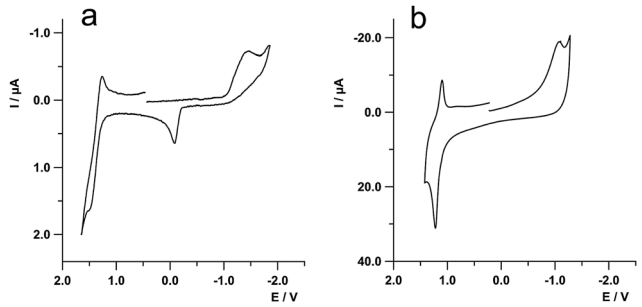


Fig. 1 Cyclic voltammetric curves of species **Chol-NO**. (a) 1 mM in 0.08 M TBAH/THF solution. Sweep rate 1 V $s^{-1}$, working electrode: Pt (125 μm, diameter), $T = 298$ K; (b) COL-NO drop-casted onto a GC disk electrode (3 mm, diameter), 0.08 M $NaBF_4$ aqueous solution with PB buffer at pH = 7.4, sweep rate 0.2 V $s^{-1}$, $T = 298$ K.

EPR spectra of **NOXs** in 1-palmitoyl-2-oleoyl-sn-glycero-3-phosphocholine (POPC) small unilamellar vesicles (SUV) at room temperature (298 K) at low microwave power (2 mW) are reported in Fig. 2, panel (f). These spectra have a lineshape much broader than that of **NOXs** in buffer solution (the spectrum of OG in buffer is reported for comparison). The broad lines are indicative of the damping of the nitroxide motion caused by its incorporation in the liposomes. **NOXs** spectra in membranes are discussed in detail in the next section.

In Fig. 2, panels (a)–(e), the saturation curves (and the corresponding fitting) for each sample in the presence of either oxygen or NiEDDA are also shown.

All the experimental details, the fitting procedure, and the used formulas are described in the Experimental section. From the fitting, the saturation parameters, $p^{i}_{1/2}$ were obtained allowing the determination of immersion depth parameters $\Phi$ (the accessibility parameters $\Pi_i$, to oxygen and to NiEDDA, were determined and reported in ESI, Table S1†). The results of the analysis are summarized in Table 2, where the reported data are the average of experiments performed at least in duplicate. The table reports the adimensional parameters $\Phi$ for standard nitroxide-labeled lipids (**SL**) and for our **NOXs** ordered by the increasing penetration depth. Overall, the data show that the water accessibility of **NOXs** decreases in the order: **Chol-NO** ≫ **DOG(L)-NO** > **DOG-NO** ≈ **OG(L)-NO** ≈ **OG-NO**.

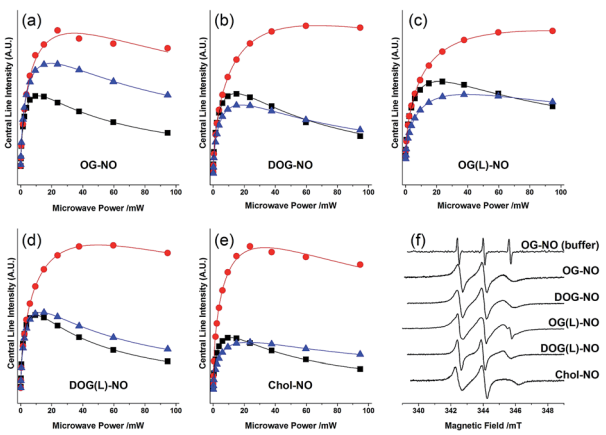


Fig. 2 Power saturation curves (dots), their fitting (lines) and EPR spectra of the **NOXs** in POPC small unilamellar vesicles acquired at room temperature (298 K) in different conditions: black squares, purged with nitrogen; red dots, in equilibrium with air (oxygen); blue triangles, 50 mM NiEDDA and purged with nitrogen. The EPR spectra are relative to the nitrogen purged samples and are taken at low microwave power. For comparison we report the spectrum of OG in buffer.

## Liponitroxides in bicelles

To fully understand, at a molecular level, the motion and orientation of **NOXs** in the bilayer, we recorded and simulated their EPR spectra in oriented lipid bicelles at near physiological temperature (308 K), Fig. 3. Bicelles have the peculiarity, with respect to micelles or vesicles, to be macroscopically oriented in solution at physiological temperature under a magnetic field, a property that makes them invaluable for the determination of

Table 2 Penetration depth parameter ($\Phi$) of the different reference spin labels (**SL**) and of the **NOXs** in POPC small unilamellar vesicles obtained at room temperature. The reported uncertainty is a rough estimate based on repeated experiments

| SL | $\Phi$ (±0.1) | NOX | $\Phi$ (±0.1) |
|---|---|---|---|
| TempoPC | <0.3[a] | **Chol-NO** | 0.7 |
| 5DPC | 1.4[b] | **DOG(L)-NO** | 1.4 |
| 7DPC | 1.2[b] | **DOG-NO** | 1.8 |
| 10DPC | 2.1 | **OG(L)-NO** | 1.9 |
| 12DPC | 2.4 | **OG-NO** | 2.1 |
| 14DPC | 3.0 | | |

[a] Repeated measurements of TempoPC showed a large variability in $\Phi$, but always lower than 0.3. [b] The apparent inversion of $\Phi$ is present also in the original paper.[15]

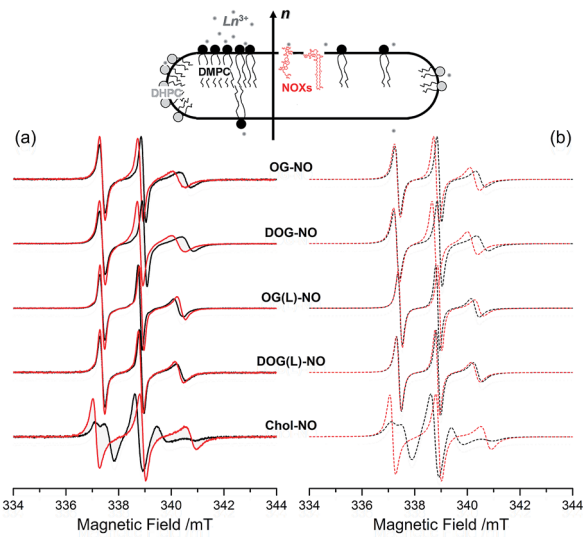


Fig. 3 Top, schematic representation of a bicelle. Panel (a), EPR spectra of **NOX** in DMPC/DHPC bicelles at 308 K. In black the spectra recorded with $B_0 \| \boldsymbol{n}$, in red the spectra recorded with $B_0 \perp \boldsymbol{n}$. Panel (b), spectral simulations (black $B_0 \| \boldsymbol{n}$; red $B_0 \perp \boldsymbol{n}$).

the order and dynamics of solutes and biological molecules in bilayers.[13,16]

These systems are composed of planar regions, made primarily by long chain phospholipids 1,2-dimyristoyl-sn-glycero-3-phosphocholine (DMPC), and of curved edge regions, composed by short-chain phospholipids, 1,2-dihexanoyl-sn-glycero-3-phosphocholine (DHPC). EPR spectra of **NOXs** in bicelles, oriented with the magnetic field ($B_0$) parallel (black line) and perpendicular (red line) to the membrane normal ($\boldsymbol{n}$), are reported in Fig. 3, panel (a). The spectral simulations, shown in dotted lines in panel (b), are in a rather good agreement with experimental data and offer some insight on the motional parameters of **NOXs** as well as on the orientation of the nitroxide moiety relative to the membrane normal; the simulation parameters are reported in Table 3. The orientation procedure and the simulation details are described in detail in the Experimental section.

The spectra show a single species in slow-motion régime, characteristic of the inclusion of the pyrroline group inside the high-viscosity membrane region. The principal values of the axial rotational diffusion tensor **D** ($\boldsymbol{D}_{\parallel} \approx \boldsymbol{D}_{\perp}$)[18] are in the order of $10^8$ $s^{-1}$, typically 1–2 order of magnitudes lower than in water and this is a clear indication that **NOXs** are fully incorporated in the bicelles. The motion of the nitroxide unit in the glycerolipids is strongly affected by the presence of the additional ethylene glycol unit. The lipids with the ethylene glycol linker (**OG(L)-NO**, **DOG(L)-NO**) have an almost isotropic motion ($\boldsymbol{D}_{\parallel} \approx \boldsymbol{D}_{\perp}$), indicating that the rotational motion of the nitroxide is almost independent from the motion of the lipid tail. On the contrary, when the nitroxide is directly attached to the glycerol unit (**OG-NO**, **DOG-NO**) the diffusion tensor is axial and typical of a molecule with a prolate shape ($\boldsymbol{D}_{\parallel} > \boldsymbol{D}_{\perp}$). The cholesterol derivative **Chol-NO** undergoes a slower and more axial motion than the glycerolipids, as expected from its bulky anisotropic shape.

A further confirmation of the inclusion of the pyrroline group inside the membrane is given by the $\boldsymbol{g}_{xx}$ and $A_{zz}$ values obtained from the simulations. These values are sensitive to the polarity of the environment and, as found by M. Plato *et al*,[17] they range from *ca.* $\boldsymbol{g}_{xx} = 2.0090$ and $A_{zz} = 3.35$ mT in an apolar environment to *ca.* $\boldsymbol{g}_{xx} = 2.0083$ and $A_{zz} = 3.65$ mT in a highly polar environment. As shown in Table 3, the obtained values clearly indicate that all **NOXs** are in an apolar environment; the $A_{zz}$ value for **Chol-NO** is larger than the others (3.45 mT *vs.* 3.35 mT, respectively), suggesting that the pyrroline moiety of this nitroxide is located in a slightly more polar environment.

The linewidths (Gaussian linewidths $\leq$0.1 mT for all spectra) are such to exclude **NOXs** clusterization that would have generated significant Lorentzian line broadening by spin–spin interaction.

As shown in Fig. 3, different spectra were recorded when bicelle planes were parallel or perpendicular to the magnetic field. This means that **NOXs** are oriented with respect to the membrane surface; with the exception of **DOG(L)-NO** which has almost completely overlapping spectra. The differences in the spectra between the two orientations depend on the degree of order experienced by the nitroxide in the bilayer: this is quantitatively expressed in Table 3 by the principal values of the adimensional, traceless, order parameter matrix $S$, in particular by the $S_{zz}$ componenent. **OG(L)-NO** and **DOG(L)-NO** have a smaller degree of order than **OG-NO** and **DOG-NO**. These results, together with the observed values for the rotational diffusion tensors, further confirm that the ethylene glycol unit decouples the motion of the pyrroline unit from that of the lipid chains. In particular, **DOG(L)-NO** has almost a negligible degree of order. On the other hand, the cholesterol derivative **Chol-NO** has a much larger degree of order than the glycerolipids and, interestingly, it displays a biaxial orientation ($S_{xx} \neq S_{yy} \neq S_{zz}$), which is typical for molecules having a strongly anisotropic shape.

EPR spectra simulations also give information about the orientation (given by the Euler angles $\Omega_D$) of the nitroxide ring relative to the principal diffusion axis ($\Omega_D$) and hence of the chain bearing the pyrroline group relative to the membrane normal. For all glycerolipids, the plane of the nitroxide ring is tilted relative to the membrane normal ($\beta_D \neq 0°$, Table 3), suggesting that the headgroup is not in a fully extended conformation. **OG(L)-NO** shows a significantly larger tilt ($\beta_D = 65°$) than the other glycerolipids ($\beta_D \sim 40°$) and this is evident in the spectra with a narrower width for the $B_0 \| \boldsymbol{n}$ orientation than for the $B_0 \perp \boldsymbol{n}$ one. The larger tilt for **OG(L)-NO** suggests that the low water accessibility of this **NOXs** (if compared with that of

Table 3 Parameters used for the fitting of the spectra of **NOXs** in bicelles. Rotational diffusion tensor ($D$), Euler angles between the magnetic and the diffusion frame ($\Omega_D$), order parameter ($S$). The $\boldsymbol{g}$ tensor for all **NOXs** is $\boldsymbol{g}_{xx} = 2.0088$; $\boldsymbol{g}_{yyx} = 2.0061$; $\boldsymbol{g}_{zz} = 2.0027$. The hyperfine tensor is $A_{xx} =$ 0.60 mT; $A_{yy} = 0.5$ mT; $A_{zz} = 3.35$ mT for all glycerolipids $A_{xx} = 0.60$ mT; $A_{yy} = 0.5$ mT; $A_{zz} = 3.45$ mT for **Chol-NO**

| | | **OG-NO** | **DOG-NO** | **OG(L)-NO** | **DOG(L)-NO** | **Chol-NO** |
|---|---|---|---|---|---|---|
| $\boldsymbol{D}/s^{-1}$ | $\boldsymbol{D}_{\parallel}$ | $3.16 \times 10^8$ | $3.16 \times 10^8$ | $1.94 \times 10^8$ | $1.94 \times 10^8$ | $4.20 \times 10^8$ |
| | $\boldsymbol{D}_{\perp}$ | $0.79 \times 10^8$ | $0.79 \times 10^8$ | $1.54 \times 10^8$ | $1.54 \times 10^8$ | $0.08 \times 10^8$ |
| $\Omega_D$[a] | $\beta$ | 42° | 40° | 65° | 40° | 90° |
| | $\gamma$ | 90° | 90° | 90° | 90° | 48° |
| $S$ | $S_{xx}$ | −0.08 | −0.10 | −0.05 | −0.015 | −0.19 |
| | $S_{yy}$ | −0.08 | −0.10 | −0.05 | −0.015 | −0.22 |
| | $S_{zz}$ | +0.16 | +0.20 | +0.10 | +0.03 | +0.41 |

[a] For an axial diffusion tensor the angle $\alpha$ is irrelevant.[18]

**DOG(L)-NO** which has the same ethylene glycol unit) is the result of the nitroxide ring folding back on the lipid chain towards the bilayer interior. For **Chol-NO**, the plane of the nitroxide ring lies perpendicular to the membrane normal ($\beta_D = 90°$) and, by considering the shape of the molecule, this suggests that the nitroxide ring is coplanar with the cholesterol rings.

### Antioxidant activity

The antioxidant activity of the synthesized **NOXs** against radical-induced lipid peroxidation was evaluated in SUV of Egg-PC containing poly-unsaturated chains susceptible of oxidation. The water-soluble azo-initiator 2,2′-azobis(2-amidinopropane) dihydrochloride (AAPH) was used as the radical generating system since it thermally decomposes at a constant rate producing a continuous flux of radicals.[19]

The water soluble nitroxide, 3-carboxy-2,2,5,5-tetramethyl-pyrroline-1-oxyl (Pyrr-NO) was included in the study for comparison.

The antioxidant activity of the synthesized lipo-nitroxides **NOXs**, and of Pyrr-NO, was evaluated by measuring the percentage inhibition of aldehydic breakdown products (Thio-barbituric Reactive Species, TBARS) formed during the peroxidation process and shown in Fig. 4. Even if TBARS assay is not so specific and may give overestimated results, it remains however the simplest, cheapest and widely used method for identifying the presence of lipid peroxide products (malondialdehyde and other aldehydes).

All synthesized compounds are able to inhibit lipid peroxidation in a percentage range 40–70%, with glycerolipid derivatives being more active than the cholesterol-functionalized analogue. A good antioxidant activity was observed also for Pyrr-NO.

### EPR signal decay

The EPR signal decay of the functionalized nitroxides incorporated in liposomes, or added to liposome suspensions as for the pyrroline nitroxide, was followed by EPR spectroscopy during incubation with AAPH at 310 K. The results are given as $h/h_0$, where $h$ is the total peak to peak intensity of the lowest line of the EPR signal at time $t$ and $h_0$ is the total peak to peak intensity of the same line at the initial time. The signal intensity decreased during incubation time as shown in Fig. 5, where typical decays are shown for **OG(L)-NO**, **Chol-NO** and Pyrr-NO nitroxides. All the glycerolipid-derivatives have a gradual decay similar to **OG(L)-NO** with the almost complete disappearance of the signal after *ca.* 1 hour without a clear delay (data not shown). The same trend was observed for the decay of **Chol-NO** EPR signal, but in this case the decay was slower and the signal disappeared in almost 2 hours.

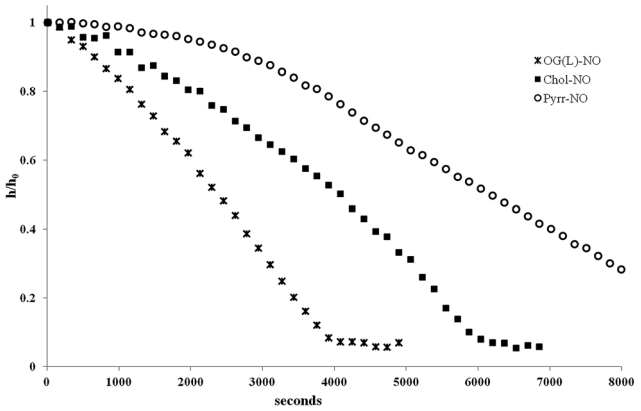


Fig. 5 Relative EPR signal intensities ($h/h_0$) *versus* time in Egg-PC liposomes loaded with nitroxides upon incubation with AAPH at 310 K. The nitroxide radical EPR signal intensity was measured as the total peak to peak intensity of the lower field peak.

On the other hand, Pyrr-NO behaved in a different way, showing a delay in the EPR signal decay. The same experiment was carried out in the absence of oxygen by degassing with argon the sample before incubation at 310 K and a gradual and more rapid decay without any delay (data not shown) was observed. For comparison, also lipid-functionalized nitroxides were incubated with AAPH in the absence of oxygen, but no differences in their EPR behaviour were observed.

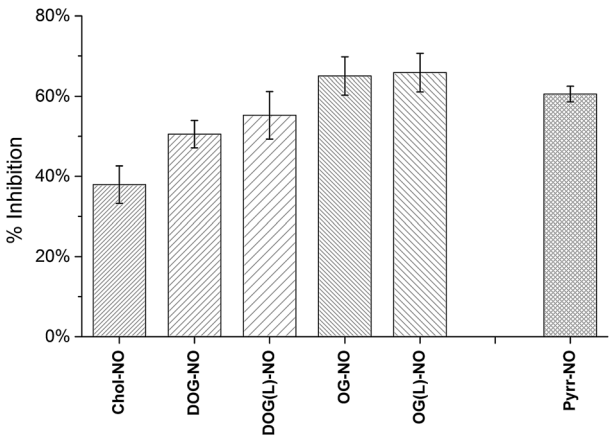


Fig. 4 % Inhibition of TBARS formation in PC (3 mM) liposomes peroxidation by **NOXs** or Pyrr-NO (0.06 mM) induced by thermal decomposition (310 K, 2 h) of AAPH (5 mM).

## Discussion

**OG-NO**, **DOG-NO**, and **OG(L)-NO** have a similar penetration depth ($\Phi \approx 2.0$) and, by comparing this value with those obtained for the **SLs**, it can be deduced that the nitroxide function in these derivatives is located between the seventh and tenth carbon of the lipid tails, well inside the bilayer. **DOG-(L)** has instead a $\Phi$ comparable to that of 5DPC, suggesting that the combination of two lipid tails with the flexible ethylene glycol unit allows it to point towards the aqueous phase. The nitroxide group of **Chol-NO** is located in the headgroup region: it has a low $\Phi$ and has a $A_{zz}$ value of 3.45 mT (Table 3), close to a typical value for a polar environment.

The different position/penetration of nitroxides can be correlated with their antioxidant activity: in Fig. 6, the %

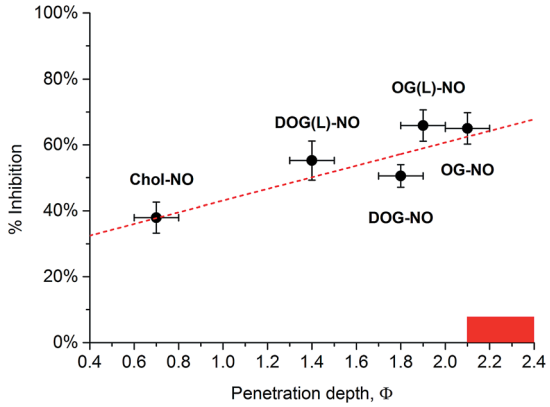


Fig. 6 Linear correlation between the % inhibition of the **NOXs** and the penetration depth. The red bar indicates the $\Phi$ value of the region C10–C12 that includes the bis-allylic carbon (C11) of PUFAs.

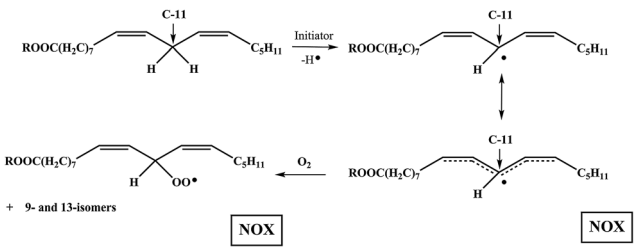


Scheme 1 Initiating steps of Egg-PC lipid peroxidation.

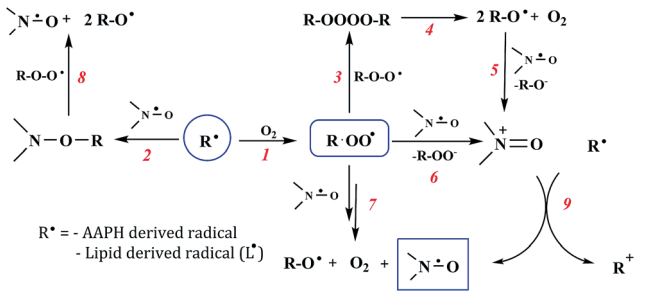


Scheme 2 Possible mechanisms of action of NOXs towards radical species involved in the process (initiation in the aqueous phase and propagation in the lipid bilayer).

inhibition of lipid peroxidation obtained in the TBARS assay is plotted as a function of the penetration depth parameter $\Phi$.

The figure shows that the antioxidant activity increases linearly with the penetration depth. The maximal activity is reached when **NOXs** are close to the most common position of the double bonds in PUFAs (red rectangle in the figure). In fact, the most active **NOXs** are located in the proximity of the bis-allylic hydrogen atoms of the linoleic chain (15% of the fatty acid residues of PC are represented by polyunsaturated linoleic acid), which are preferentially abstracted by radical initiators (peroxyls, alkoxyls, *etc.*) in the first step of LP (Scheme 1). This is in agreement with data reported in the literature according to which nitroxides work as better inhibitors in the peroxidation of rat liver microsomes[7c] if they are at the same depth of the generated radicals in the bilayer.

Peroxyl radicals are usually considered as initiators of LP. In the present work, they are initially formed in the aqueous phase by the rapid reaction between AAPH-derived C-centred radicals and oxygen (the coupling is nearly diffusion controlled, $k \simeq 10^9$ $M^{-1}$ $s^{-1}$). They are able to cross the lipid membrane and to abstract a labile hydrogen atom from a lipid chain giving the corresponding C-centred radical L$^\bullet$ in the propagation step ($k =$ 16 $M^{-1}$ $s^{-1}$).[20] Alternatively, alkylperoxyl radicals may also dimerize to give the corresponding unstable tetraoxide which, in turn, decomposes with formation of molecular oxygen and of the corresponding alkoxyls ($k \simeq 10^5$ $M^{-1}$ $s^{-1}$ in water), as evidenced by spin trapping experiments,[21] (reactions 3 and 4 in Scheme 2), able to initiate lipid peroxidation and to generate L$^\bullet$ radicals, as well. LP process has thus been triggered and **NOXs**, being incorporated in the membrane interior, might act as chain-breaking antioxidants by reacting with the lipid-derived C-radicals (L$^\bullet$) through a fast radical coupling[22] or with the corresponding O-centred radicals (peroxyls LOO$^\bullet$ and alkoxyls LO$^\bullet$ formed in the bilayer from the reaction of L$^\bullet$ with oxygen) though an electron transfer process.[10a] At physiological temperature and $pO_2$, the concentration of L$^\bullet$ should be lower than that of LOO$^\bullet$, hence the reaction between **NOXs** and alkyl radicals should be disfavoured with respect to that with oxygen-centred ones. However, a competition between nitroxides and oxygen towards L$^\bullet$ radicals cannot be ruled out, although oxygen is about four times more concentrated in membranes than in aqueous phases.[23] In fact, the reaction rate between L$^\bullet$ and $O_2$ to yield LOO$^\bullet$ does not depend only on oxygen partition but also on its diffusion, which is *ca.* 10 times slower in lipid bilayer than in water.

Lipid-functionalized nitroxides could in principle react both with C-centred radicals (L$^\bullet$) and O-centred radicals derived from AAPH, or generated from the lipid chains (LO$^\bullet$ and LOO$^\bullet$), but all these reactions have to be considered on the basis of the redox potentials of the **NOXs**.

Focusing on the oxidation potentials listed in Table 1 for **NOXs** and the redox potentials reported for peroxyl radicals,[24] an electron transfer process[25] (reaction 6, Scheme 2) is rather unlikely to occur in a lipidic environment especially if an "outer sphere" single electron transfer mechanism is considered. More favorable is the reaction when the oxidizing species are alkoxyl radicals (reaction 5, Scheme 2) instead of peroxyls due to their higher reduction potentials.[24] However, it cannot be excluded that the reaction between **NOXs** and O-centred radicals (peroxyls and alkoxyls) proceeds according to an inner-sphere electron transfer mechanism.[10a]

On the other hand, if the reactions reported in Scheme 2 are considered from a kinetic point of view, we can observe that once the initiating C-centred radicals are formed (R$^\bullet$ could derive from AAPH in the aqueous phase or from the lipid chains inside the membrane), they may react either with molecular oxygen or with **NOXs** (reactions 1 and 2, respectively). A competition between the two reactions is possible, both processes being characterized by very high rate constants near

to the diffusion control limit in liquid solutions. However, it has been reported that in the system under investigation, water-soluble peroxyl radicals are generated from AAPH decomposition approximately at a rate of $10^{-8}$–$10^{-9}$ M $s^{-1}$,[26] thus representing the rate determining step for the whole process. In fact, all the rate constants for the reactions reported in the scheme should be 3–4 order of magnitude higher and very close to each other,[27] and could occur with the same probability. The formed peroxyls may thus undergo self-decomposition (reactions 3 and 4) to give the corresponding alkoxyls, able to propagate the oxidative process by a H-abstraction from lipid chains ($k_{abs} \approx 10^5$ $M^{-1}$ $s^{-1}$), or to be reduced by nitroxides (reaction 5). In this latter reaction, as well in reaction 6, oxoammonium cations are formed which are known to be strong oxidants, able to react with alkyl radicals as indicated in reaction 9.[28]

The minor protection effect against lipid peroxidation observed for the cholesterol-derivative may be likely explained considering its location close to the membrane surface, far away from the site of generation of L$^{\bullet}$ radicals. **Chol-NO** could thus react with the initiators radicals (O-centred ones) formed by AAPH, before they reach the oxidable lipid chain. Moreover, **Chol-NO** has a reduced mobility inside the membrane due to its rigid structure and liposomes viscosity as well. As a consequence, the initiating radicals generated in the aqueous phase are only partially intercepted by the antioxidant and can thus propagate the peroxidation of the lipid bilayers. In fact, only a small fraction of attacking radicals is sufficient to induce chain oxidation of many lipid molecules.

The good antioxidant activity of Pyrr-NO, comparable with those of the glycerolipid functionalized nitroxides and better than that of **Chol-NO**, may be explained considering its location in the water phase, where the initiating radicals are generated and where the reaction (electron transfer) is expected to occur. In fact, as shown in Table 1 or reported in the literature,[14] the pyrroline moiety is more easily oxidized in an aqueous environment even by peroxyl radicals: a rate constant of $8.1 \times 10^5$ $M^{-1}$ $s^{-1}$ has been reported[10a] for the reaction between 3-carbamoylproxyl nitroxide and *t*-butylperoxyl radicals in aqueous solution. Similar or even higher rate constants (according to their reduction potentials[24]) are expected for the reduction of an alkoxy radical by a nitroxide.

EPR measurements of **NOXs** signal decay indicate that the disappearance of the signal is gradual, with no delay, and rather slow likely because of the occurrence of reactions 7, 8 and 9 (Scheme 2).[9,29] The even slower decay observed with **Chol-NO** compared to that of the other glycerolipid nitroxides can be justified by its localization and lower mobility within the bilayer[30] and is in agreement with its lower antioxidant activity. The presence of a delay in the Pyrr-NO signal decay indicates that during this time interval it reacts very slowly with O-centred radicals[7e,31] generated from AAPH and, once the oxygen dissolved in solution has been consumed, Pyrr-NO reacts with AAPH derived C-centred radicals (reaction 1, Scheme 2). This latter reaction accounts also for the fact that the signal decay was faster in the absence of oxygen and with no delay. On the other hand, since no differences were observed with **NOXs**, in the presence or in the absence of oxygen, it could be hypothesized that with these derivatives the coupling of the nitroxide with C-centred radicals formed from AAPH and from the lipid chains represents the main reaction.

According to the TBARS assay, glycerolipid nitroxides and Pyrr-NO seem to have the same antioxidant activity, whereas EPR signal decays are rather different. This could be explained by considering the differences between the two kinds of experiments. As already said, TBARS assays allow the determination of the final aldehydic products of LP without considering the fate of the antioxidant, *i.e.* the nitroxide in the present work. On the other hand, when EPR measurements are performed, the disappearance of the nitroxide is monitored and hence we have direct information on the nitroxide, on its reactivity and on its fate. **NOXs** in liposomes are consumed faster than Pyrr-NO in the water phase and this may likely be due to the fact that Pyrr-NO may react only with O-centred radicals, whereas **NOXs** react both with C- and O-centred radicals. Moreover, the radicals present in the aqueous phase are those deriving from the slow decomposition of the azo-initiator, while in the lipid environment where peroxidation, a radical chain process, is occurring we can expect that the number of radical species should be higher.

## Conclusions

The antioxidant activity of nitroxides functionalized with cholesterol or glycerol units **NOXs** has been studied and correlated with their penetration into POPC liposomes chosen as model membranes. **NOXs** are selectively incorporated at different depths in the bilayer in close proximity to the site of damage during lipid peroxidation. Those derivatives which are closer to the oxidable carbon atoms of the lipid chains are better inhibitors of lipid peroxidation.

Moreover, the obtained results indicate that nitroxides may behave differently according to their localization. In particular, they can be seen as preventive or chain-breaking antioxidants according to their environment and to their penetration attitude within the bilayer. **Chol-NO**, which is inserted in the membrane but close to the surface, can scavenge initiating radicals but not the lipophilic radicals formed during the propagation steps and hence is not able to break the chain propagation. On the other hand, the glycerol nitroxides residing deeper in the membrane interior may not only block the initiating radicals but may also be regarded as chain-breaking antioxidants, being able to intercept the radicals responsible for the propagation of the lipid peroxidation. This is of particular interest since the antioxidant activity often depends more on the localization than on the chemical reactivity.

As a concluding remark, we point out that our approach is based on the combination of advanced experimental techniques that allowed us to probe the properties of these system in-depth. Nevertheless, in modern EPR spectroscopy, there is not only a trend towards to the use of DFT methods for the evaluation of the EPR parameters,[32] but also to the integration of spectroscopic data, DFT and molecular dynamics to better characterize the effects of the molecular motions in different environments.[33] Despite the availability of these methods, they

have not been applied yet to refine the interpretation of EPR data in complex environments such as biological membranes, and we think that this approach could represent an interesting development in this field.

## Experimental section

All materials and reagents used in the synthesis of **NOXs** were purchased from Sigma-Aldrich and used without purification. 2,2,5,5-Tetramethyl-3-pyrrolin-1-oxyl-3-carboxilic acid (Pyrr-NO) was prepared according to the method of Rozanstev.[34]

$^1$H NMR spectra and $^{13}$C NMR spectra were recorded on a Varian Mercury 400 (400 MHz and 100 MHz, respectively) at 25 °C after *in situ* reduction with hydrazobenzene. Chemical shifts ($\delta$) are given in ppm and residual solvent signals for $CHCl_3$ ($\delta_H$ 7.26 ppm and $\delta_C$ 77.0 ppm) were used as internal references. Coupling constants ($J$) are given in Hertz. Electron spray ionization mass spectrometry (ESI-MS) was performed on an Agilent Series 1100 MSD Mass Spectrometer. High resolution mass spectrometry was performed on a Xeno G2-S QTof Waters spectrometer. Elemental analysis was performed on a Thermo Fischer Scientific FLASH 2000 Organic Elemental Analyzer. FTIR spectra were acquired using DRIFT technique on a Perkin Elmer Spectrum GX1 and are expressed in wave number ($cm^{-1}$).

Tetrabutylammonium hexafluorophosphate (TBAH), sodium tetrafluoborate ($NaBF_4$) and phosphate buffer solution (PB) were used as received as supporting electrolyte, and all were electrochemical or analytical grade from Sigma-Aldrich. Water was milliQ grade. Dry tetrahydrofuran (THF) was purified and dried as previously reported,[35] stored in a specially designed Schlenk flask and protected from light.

Shortly before performing the electrochemical measurements, the solvent was distilled *via* a closed system into an electrochemical cell containing the supporting electrolyte and the species under examination.

1-Palmitoyl-2-oleoyl-sn-glycero-3-phosphocholine (POPC), 1,2-dihexanoyl-sn-glycero-3-phosphocholine (DHPC), 1,2-dimyristoyl-sn-glycero-3-phosphocholine (DMPC) and all nitroxide-labeled phospholipids (**SLs**): 1-palmitoyl-2-stearoyl-(*n*-doxyl)-sn-glycero-3-phosphocholines (5DPC, 7DPC, 10DPC, 12DPC and 14DPC) and 1-palmitoyl-2-oleoyl-sn-glycero-3-phospho(tempo)-choline (TempoPC) were purchased from Avanti Polar Lipids (Alabaster, AL, USA) as chloroform solutions. Nickel(II)-ethylene-*N*,*N*′ diaminediacetic acid (NiEDDA) was prepared from ethylenediamine-*N*,*N*′-diacetic acid (EDDA) and nickel(II) hydroxide [$Ni(OH)_2$] according to published procedures.[15] These reagents, 2-[4-(2-hydroxyethyl)-1-piperazinyl] ethanesulfonic acid (HEPES), and the lanthanide salts $TmCl_3 \cdot 6H_2O$ and $DyCl_3 \cdot 6H_2O$ were purchased from Sigma-Aldrich. A 50 mM, pH 7.0, HEPES buffer solution was prepared to be used for the preparation of POPC small unilamellar vesicles (SUV) and bicelles, and for the stock solutions of $Tm^{3+}$ and $Dy^{3+}$.

Egg-yolk L-α-phosphatidylcholine (Egg-PC) as chloroform solution for liposomes preparation was purchased from Sigma-Aldrich and used without purification. A 5 mM phosphate buffer (PB) solution was prepared to be used for PC liposomes, for Pyrr-NO and AAPH solutions.

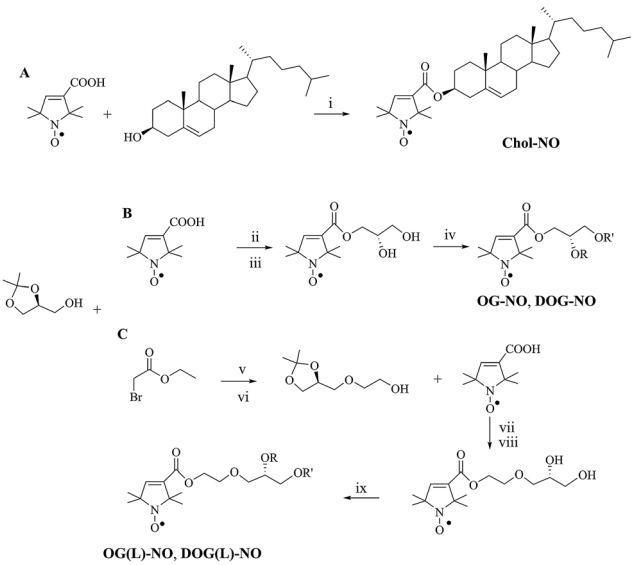


Scheme 3 Reagents and conditions: (A) (i) DCC, DMAP, dry DCM, rt, on, 63%. (B) (ii) DCC, DMAP, DCM, rt, on, 51%. (iii) *p*-TsOH, $CH_3OH$, rt, on, 72%. (iv) Oleic acid (1 or 2 eq.), DCC, DMAP, DCM, rt, on, 50% (**OG-NO**), 88% (**DOG-NO**). (C) (v) NaH (60%), dry THF, 0 °C then rt, on, 40%. (vi) $LiAlH_4$, dry THF, 0 °C, 83%. (vii) DCC, DMAP, DCM, rt, on, 62%. (viii) *p*-TsOH, $CH_3OH$, rt, on, 72%, 98%. (ix) Oleic acid (1 or 2 eq.), DCC, DMAP, DCM, rt, on, 40% (**OG-(L)-NO**), 67% (**DOG(L)-NO**).

### Synthesis

**Chol-NO** was synthesized by *N*,*N*-dicyclohexylcarbodiimide (DCC) coupling of a cholesterol molecule with 2,2,5,5-tetramethyl-3-pyrrolin-1-oxyl-3-carboxylic acid Pyrr-NO (Scheme 3A). Glycerolipid nitroxides were synthesized following a synthetic procedure already reported in the literature.[36] (Scheme 3B and C), starting from 1,2-isopropyliden-3-*O*-sn-glycerol.

For **OG-NO** and **DOG-NO**, it was condensed with Pyrr-NO and, after removal of the isopropylidene protecting, was esterified with one (**OG-NO**) or two equivalents of oleic acid (**DOG-NO**). **OG(L)-NO** and **DOG(L)-NO** were prepared with the same reactions, but in these cases 1,2-isopropyliden-3-*O*-sn-glycerol was first reacted with ethyl bromoacetate in order to introduce the oxyethylene linker.

Spectroscopic characterization of the synthesized **NOXs** can be found in the ESI.†

### Electrochemical measurements

Electrochemical experiments were carried out in an airtight single-compartment cell described elsewhere[37] by using platinum and glassy carbon (GC) as working electrode, a platinum spiral as counter electrode and a silver spiral as a quasi-reference electrode. For the measurements in aprotic solvent, the cell containing the supporting electrolyte and the electroactive compound was dried under vacuum at about 110 °C for at least 48 h before each experiment. All the $E_{1/2}$ potentials have been directly obtained from CV curves as averages of the cathodic and anodic peak potentials for one-electron peaks and by digital simulation for those processes closely spaced in

 

multielectron voltammetric peaks. The $E_{1/2}$ values are referred to a normal hydrogen electrode (NHE) and have been determined by adding, at the end of each experiment, ferrocene as an internal standard and measuring them with respect to the ferrocenium/ferrocene couple standard potential. The potentials thus obtained were not corrected for the two unknown contribution of the liquid junction potential between the organic phase and the aqueous NHE solution. Experiments in aqueous solution of the species immobilized as film, onto the electrode surface, have been carried out in the same cell described above. The species were immobilized on the GC working electrode (3 mm diameter disk) as thin film by drop-casting 100 μL of a 0.1 mM chloroform solution of the compounds investigated.

Voltammograms were recorded with an AMEL Mod. 552 potentiostat or a custom made fast potentiostat[38] controlled by an AMEL Mod. 568 programmable function generator. The potentiostat was interfaced to a Nicolet Mod. 3091 digital oscilloscope and the data transferred to a personal computer by the program Antigona.[39] Minimization of the uncompensated resistance effect in the voltammetric measurements was achieved by the positive-feedback circuit of the potentiostat. Digital simulations of the cyclic voltammetric curves were carried out either by Antigona or DigiSim 3.0.

### Penetration depth measurements

Penetration depth experiments were performed in POPC SUV prepared by mixing the chloroform stock solutions of POPC and NOXs or SLs in a 100 : 1 ratio. The mixed solutions were evaporated in a glass test tube under a stream of dry nitrogen gas and the resulting film was dried overnight under vacuum. The lipid film was hydrated for 30 minutes with HEPES buffer to a final concentration of 10 mM for the lipid and 100 μM for NOX or SL. Lipid suspensions were sonicated in a water bath until they started to clear. SUV in the 30–50 nm diameter range were obtained and their dimensions were checked during preparation by Dynamic Light Scattering (DLS) using a NICOMP Model 370 Submicron Particle Sizer by Pacific Scientific. Vesicles were used fresh after preparation.

The EPR experiments were performed using a Bruker ESP380 spectrometer operating at X-band (~9.5 GHz), equipped with a room-temperature dielectric resonator, ER4123D. The microwave frequency was measured by a frequency counter, HP5342A. All spectra were obtained using the following parameters: modulation amplitude 0.16 mT; modulation frequency 100 kHz; time constant 41 ms; conversion time 82 ms; scan width 1.25 mT; 512 points; temperature 298 K. The microwave power was ramped down automatically from 95 mW to 0.05 mW (the attenuation ramp in dB units was 2.0, 4.0, 6.0, 8.0, 10.0, 12.0, 14.0, 16.0, 18.0, 20.0, 25.0, 30.0, 35.0). The spectra were acquired in a single scan. The experimental protocol for the insertion depth measurements is as follows. Approximately 5 μL of sample were loaded into a gas-permeable TPX capillary (L&M EPR Supplies, Inc., Milwaukee, WI, USA) and three saturation experiments were performed. The first experiment was done on the sample in equilibrium with air to saturate the membrane with oxygen. The second experiment was performed on the same sample after de-oxygenation under a dry nitrogen flow for twenty minutes. The third experiment was performed on a new sample to which NiEDDA was added to a final concentration of 50 mM; the sample was then de-oxygenated as above. All experiments were performed at least in duplicate. The power saturation data were obtained using a home-written program in Matlab that calculates the peak-to-peak amplitudes of the central line of the spectra. The saturation curves were obtained plotting the amplitude data *vs.* the microwave power, and fitted using the standard equation:[15]

$$y = Ap_{1/2}[1 + (2^{1/h} - 1)x/p_{1/2}]^{-h}$$

$p_{1/2}$ is the saturation parameter, namely the power where the first derivative amplitude is reduced to half of its unsaturated value, $h$ is the homogeneity parameter, indicating the homogeneity of saturation of the resonance line, (ranging between $h = 1.5$ for a fully homogeneously-broaden line and $h = 0.5$ for a fully inhomogeneously-broaden line), and $A$ is a scaling factor that accounts for the absolute signal intensity. The saturation profile and the saturation parameter were obtained also for DPPH (2,2-diphenyl-1-picrylhydrazyl).[40] The best-fit $p_{1/2}$ parameters of the three experiments described above were used to calculate the dimensionless immersion depth parameter ($\Phi$) as

$$\Phi = \ln \frac{p_{1/2}^{\text{oxygen}} - p_{1/2}^{\text{nitrogen}}}{p_{1/2}^{\text{NiEDDA}} - p_{1/2}^{\text{nitrogen}}}$$

### Bicelle stock preparation and EPR experiments

Chloroform solutions of the phospholipids (DMPC and DHPC) and a methanol solution of the **NOX** were mixed in a glass test tube in a 1 : 100 **NOX** to DMPC ratio. The obtained solutions contained 11.2 μmol of DMPC, 3.1 μmol of DHPC, and, where present, 25 nmol of **NOX** (~0.2% of the total lipids); the $q$ = [DMPC]/[DHPC] ratio was therefore $q \sim 3.5$. A thick lipid film was produced by evaporation of the solvent under a stream of dry nitrogen gas which was then dried under vacuum overnight. The following day the lipids were scratched off the glass tube and placed into an Eppendorf tube, to which 33 μL of buffer were added, obtaining a 25% (w/w) lipid concentration. The resulting suspension was vortexed until it appeared homogeneous. The sample was then placed in a bath sonicator that was filled with an ice/water mixture and sonicated for 30 minutes. Finally, the solution was subjected to four freeze/thaw cycles: 30 minutes in a 328 K water bath followed by a quick freeze in liquid nitrogen; vortexing of the sample at each step was performed to insure perfect homogeneity. The procedure yielded a clear, viscous, stock of bicelles with the **NOX** incorporated in the bilayers. Starting from the stock solution, 25 μL were prepared as follows: 15 μL of bicelles were added to 10 μL of buffer (for isotropic samples), or, for oriented samples, to 10 μL of buffered lanthanide solution of $Tm^{3+}$ or $Dy^{3+}$ (corresponding to a final $[Ln^{3+}]$/[DHPC] ratio of 0.1). The resulting solution was transferred to a 1 mm inner diameter EPR quartz tube. The final concentration of the phospholipids was 17% (w/w). Given the

experimental conditions (lipid concentration, $q$ ratio, temperature), the bicelles used in this work are not ideal disks, but rather stacks of almost planar phospholipid bilayers dotted with DHPC pores and separated by buffer regions ~15 nm wide.[41]

Samples with $\boldsymbol{n}$ oriented along and perpendicular to the magnetic field can be obtained in two ways: (a) by preparing two samples doped with lanthanide salts that yield bicelles with different orientation in a strong magnetic field ($B_0$), $Tm^{3+}$ for $\boldsymbol{n} \| B_0$ or $Dy^{3+}$ for $\boldsymbol{n} \perp B_0$; (b) by preparing a single sample doped with $Tm^{3+}$ and taking the spectra before and after a rotation of the sample tube by 90° inside the cavity of the spectrometer. This latter method exploits the extremely high viscosity of the bicelle solution at 308 K and the slow relaxation of the oriented phase at the magnetic field of the experiment (350 mT) which prevents the lipid reorientation within the timeframe of the EPR experiments (3 minutes). After having verified the equivalence of the procedures, the second method was adopted in this work since it requires a single sample.

A literature procedure[13] was used to obtain aligned samples: the sample tube was placed at room temperature (~298 K) in the EPR cavity and the magnetic field was set to 800 mT; then the temperature was slowly raised to 318 K and subsequently lowered to the temperature of choice, 308 K (35 °C). The magnetic field was set to ~350 mT and the spectrum was recorded immediately: loss of order in the sample during the measurement time (~40 s) is negligible as a result of the high viscosity of the bicelle solution and slow relaxation of the oriented phase at the magnetic field of the experiment (350 mT) which prevents the lipid reorientation.

EPR spectra were performed using a Bruker ER200D spectrometer operating at X-band (~9.5 GHz), equipped with a rectangular cavity, ER4102ST, fitted with a cryostat, and a variable-temperature controller, Bruker ER4111VT; the microwave frequency was measured by a frequency counter, HP5342A. All spectra were obtained using the following parameters: microwave power 2.1 mW; modulation amplitude 0.16 mT; modulation frequency 100 kHz; time constant 20 ms; conversion time 41 ms; scan width 15 mT; 1024 points; temperature 308 K; all spectra were obtained in a single scan.

### EPR spectral simulations

We performed simulations of the **NOX** spectra with a program based on the stochastic Liouville equation,[18] that is extensively used to simulate EPR spectra of spin-labeled systems.[16d,42] The simulation method relies on several reference systems whose relative orientation is defined by different sets of Euler angles.[18] The simulation parameters are listed in Table 3. The principal values of the $\boldsymbol{g}$ and $^{14}N$ hyperfine ($A$) tensors were obtained from the literature;[16d,43] the principal values of the rotational diffusion tensor ($\boldsymbol{D}$), the relative orientation of its principal axes relative to the $\boldsymbol{g}$ tensor reference frame ($\Omega_D$), the adimensional and traceless order parameter matrix ($S$, expressing the degree of order), and the angle ($\Psi$) defining the orientation of the magnetic field relative to the average long diffusion axis were obtained from the simulation.

### Peroxidation of Egg-PC liposomes and assessment of nitroxides % inhibition (TBARS assay): oxidation induced by 2,2′-azobis(2-amidinopropane) dihydrochloride (AAPH)

Liposomes were prepared by the "thin film hydration" method. Chloroform stock solutions (2 mM) were prepared for each tested compound except for 2,2,5,5-tetramethyl-3-pyrrolin-1-oxyl-3-carboxilic acid (Pyrr-NO), whose 2 mM solution was prepared in phosphate buffer PB. Appropriate amounts of chloroform solutions of PC (100 mg $mL^{-1}$) and tested compound (2 mM in $CHCl_3$) were mixed in a 50 : 1 molar ratio. The solvent was slowly evaporated with a stream of nitrogen and the thin film obtained was dried for at least 2 h under reduced pressure. This dried film was then resuspended by vortex agitation in the required amount of 5 mM PB (pH 7.4) to a 3 mM Egg-PC and 0.06 mM antioxidant final concentration and incubated overnight to swell and stabilize. The same procedure was used to prepare a suspension of Egg-PC liposomes (3 mM final concentration) without tested nitroxides to be used as the control in the evaluation of the percentage of inhibition of nitroxides on the basis of the equation below. Samples containing Pyrr-NO were obtained by hydrating the Egg-PC film with a PB- solution containing the proper volume of the 2 mM stock solution in PB in order to have 0.06 mM final concentration of nitroxide. The resulting MLV (Multi Lamellar Vesicles) were sonicated for 12 min with a Sonic Vibracell sonicator to obtain SUV (Small Unilamellar Vesicles) and the size distribution (mean diameter) was verified by Dynamic Light Scattering (DLS) using a Nanosizer (Nano-ZS, Nanoseries, Malvern) and found to be in the range 89–105 nm. Oxidized samples were obtained by taking up 300 μL portions of each dispersion, adding 25 μL AAPH 65 mM (5 mM final concentration) and incubating for 2 h at 310 K. Addition of 10 μL of 20 mM methanolic BHT to the oxidized liposomes stopped the reaction and prevented further Egg-PC peroxidation during the TBARS assay. Other 300 μL of the liposome dispersions were added with 25 μL of PBS (instead of AAPH) and 10 μL of 20 mM methanolic BHT to make sure that during incubation, also in the absence of radical initiator, no oxidation occurs and incubated at 310 K for the same time. 0.9 mL of TBA–TCA–HCl reagent (0.375% w/v TBA, 15% w/v TCA, 0.2 M HCl) were added to all samples, oxidized and non-oxidized, which were then heated for 15 min at 368 K, cooled and centrifugated at 5000 rpm for 10 min. A pink chromophore developed after the reaction between the thiobarbituric acid and malondialdehyde and other aldehydes formed from the degradation of lipid peroxides. Its absorbance was measured at 532 nm on a microplate reader (Biotek, Synergy HT) for the determination of the aldehydic breakdown products of lipid peroxidation (TBARS).[44] The antioxidant activity of the studied compounds was expressed as % inhibition according to the following equation:

$$\%\ \text{Inhibition} = (1 - \Delta A_{\text{sample}}/\Delta A_{\text{PC}}) \times 100$$

where $\Delta A_{\text{sample}}$ is the difference of the absorbance between the oxidized and non-oxidized sample containing nitroxide and $\Delta A_{\text{PC}}$ is the difference of the absorbance between the oxidized

 

and non-oxidized Egg-PC. All experiments were run in triplicate and repeated at least four times.

### EPR signal decay

SUV were prepared from PC and **NOX** (2 mM in $CHCl_3$) or Pyrr-NO (2 mM in PB) following the same procedure described for AAPH experiments. 25 μL of AAPH (final concentration 5 mM) were added to 300 μL of each suspension in an Eppendorf tube, mixed and transferred into a glass capillary tube which was then put inside the EPR cavity. Each sample was incubated for 2 h at 310 K following the decay of the nitroxide three lines signal upon heating. EPR spectra were recorded using a Bruker EMX spectrometer operating at X-band (~9.5 GHz), equipped with a rectangular cavity, ER4102ST, fitted with a variable-temperature controller, a microwave frequency counter and an NMR gaussmeter for field calibration. Spectra were recorded using the following parameters: microwave power 20 mW; modulation amplitude 0.2 mT; modulation frequency 100 kHz; time constant 0.32 ms; conversion time 41 ms; scan width 10 mT; number of scans 50; delay after each measurement 120 s.

## Acknowledgements

We thank Dr Barbara Biondi for ESI-MS spectra. This work was supported by MIUR (PRIN 2010–2011) [2010PFLRJR(PROxi); 2010NRREPL; 2010A2FSS9] and by Fondazione CARIPARO (Progetti Eccellenza 2011/2012).

## References

1 A. Negre-Salvayre, N. Auge, V. Ayala, H. Basaga, J. Boada, R. Brenke, S. Chapple, G. Cohen, J. Feher, T. Grune, G. Lengyel, G. E. Mann, R. Pamplona, G. Poli, M. Portero-Otin, Y. Riahi, R. Salvayre, S. Sasson, J. Serrano, O. Shamni, W. Siems, R. C. M. Siow, I. Wiswedel, K. Zarkovic and N. Zarkovic, *Free Radical Res.*, 2010, **44**, 1125.

2 M. C. Krishna and A. Samuni, *Methods Enzymol.*, 1994, **234**, 580.

3 (*a*) V. W. Bowry and K. U. Ingold, *J. Am. Chem. Soc.*, 1992, **114**, 4992; (*b*) A. Samuni, S. Goldstein, A. Russo, J. B. Mitchell, M. C. Krishna and P. Neta, *J. Am. Chem. Soc.*, 2002, **124**, 8719; (*c*) S. Goldstein, A. Samuni and A. Russo, *J. Am. Chem. Soc.*, 2003, **125**, 8364.

4 (*a*) M. C. Krishna, D. A. Grahame, A. Samuni, J. B. Mitchell and A. Russo, *Proc. Natl. Acad. Sci. U. S. A.*, 1992, **89**, 5537; (*b*) M. C. Krishna, A. Russo, J. B. Mitchell, S. Goldstein, H. Dafni and A. Samuni, *J. Biol. Chem.*, 1996, **271**, 26026.

5 M. C. Krishna, A. Samuni, J. Taira, S. Goldstein, J. B. Mitchell and A. Russo, *J. Biol. Chem.*, 1996, **271**, 26018.

6 P. Bar-On, M. Mohsen, R. Zhang, E. Feigin, M. Chevion and A. Samuni, *J. Am. Chem. Soc.*, 1999, **121**, 8070.

7 (*a*) G. Cighetti, P. Allevi, S. Debiasi and R. Paroni, *Chem. Phys. Lipids*, 1997, **88**, 97; (*b*) A. N. Cimato, L. L. Piehl, G. B. Facorro, H. B. Torti and A. A. Hager, *Free Radicals Biol. Med.*, 2004, **37**, 2042; (*c*) Y. Miura, H. Utsumi and A. Hamada, *Arch. Biochem. Biophys.*, 1993, **300**, 148; (*d*) U. A. Nilsson, L. I. Olsson, G. Carlin and A. C. Bylund-Fellenius, *J. Biol. Chem.*, 1989, **264**, 11131; (*e*) A. M. Samuni and Y. Barenholz, *Free Radicals Biol. Med.*, 1997, **22**, 1165; (*f*) A. M. Samuni and Y. Barenholz, *Free Radicals Biol. Med.*, 2003, **34**, 177; (*g*) T. Yamasaki, Y. Ito, F. Mito, K. Kitagawa, Y. Matsuoka, M. Yamato and K. Yamada, *J. Org. Chem.*, 2011, **76**, 4144.

8 (*a*) J. Antosiewicz, E. Damiani, W. Jassem, M. Wozniak, M. Orena and L. Greci, *Free Radicals Biol. Med.*, 1997, **22**, 249; (*b*) E. Damiani, R. Castagna and L. Greci, *Free Radicals Biol. Med.*, 2002, **33**, 128.

9 P. Stipa, *J. Chem. Soc., Perkin Trans. 2*, 2001, 1793.

10 (*a*) S. Goldstein and A. Samuni, *J. Phys. Chem. A*, 2007, **111**, 1066; (*b*) D. H. R. Barton, V. N. le Gloahec and J. Smith, *Tetrahedron Lett.*, 1998, **39**, 7483.

11 B. P. Soule, F. Hyodo, K.-I. Matsumoto, N. L. Simone, J. A. Cook, M. C. Krishna and J. B. Mitchell, *Free Radicals Biol. Med.*, 2007, **42**, 1632.

12 (*a*) S. Banerjee, U. R. Desai and G. K. Trivedi, *Tetrahedron*, 1992, **48**, 133; (*b*) S. Banerjee and G. K. Trivedi, *Tetrahedron*, 1992, **48**, 9939; (*c*) S. Banerjee, G. K. Trivedi, S. Srivastava and R. S. Phadke, *Bioorg. Med. Chem.*, 1993, **1**, 341; (*d*) S. Banerjee, G. K. Trivedi, S. Srivastava and R. S. Phadke, *Steroids*, 1994, **59**, 377–382; (*e*) R. Katoch, G. K. Trivedi and R. S. Phadke, *Bioorg. Med. Chem.*, 1999, **7**, 2753; (*f*) S. Pajk and S. Pečar, *Tetrahedron*, 2009, **65**, 659.

13 T. B. Cardon, E. K. Tiburu and G. A. Lorigan, *J. Magn. Reson.*, 2003, **161**, 77.

14 P. Carloni, E. Damiani, L. Greci, P. Stipa, G. Marrosu, R. Petrucci and A. Trazza, *Tetrahedron*, 1996, **52**, 11257.

15 C. Altenbach, D. A. Greenhalgh, H. G. Khorana and W. L. Hubbell, *Proc. Natl. Acad. Sci. U. S. A.*, 1994, **91**, 1667.

16 (*a*) M. Bortolus, A. Dalzini, C. Toniolo, K. S. Hahm and A. L. Maniero, *J. Pept. Sci.*, 2014, **20**, 517; (*b*) M. Bortolus, M. de Zotti, F. Formaggio and A. L. Maniero, *Biochim. Biophys. Acta, Biomembr.*, 2013, **1828**, 2620; (*c*) M. Bortolus, G. Parisio, A. L. Maniero and A. Ferrarini, *Langmuir*, 2011, **27**, 12560; (*d*) J. J. Inbaraj, T. B. Cardon, M. Laryukhin, S. M. Grosser and G. A. Lorigan, *J. Am. Chem. Soc.*, 2006, **128**, 9549.

17 M. Plato, H. J. Steinhoff, C. Wegener, J. T. Torring, A. Savitsky and K. Mobius, *Mol. Phys.*, 2002, **100**, 3711.

18 D. E. Budil, S. Lee, S. Saxena and J. H. Freed, *J. Magn. Reson., Ser. A*, 1996, **120**, 155.

19 E. Niki, *Methods Enzymol.*, 1990, **186**, 100.

20 F. Antunes, L. R. C. Barclay, M. R. Vinqvist and R. E. Pinto, *Int. J. Chem. Kinet.*, 1998, **30**, 753.

21 (*a*) A. G. Krainev and D. J. Bigelow, *J. Chem. Soc., Perkin Trans. 2*, 1996, 747; (*b*) R. U. Rojas Wahl, L. Zeng, S. A. Madison, R. L. de Pinto and B. J. Shay, *J. Chem. Soc., Perkin Trans. 2*, 1998, 2009.

22 A. L. J. Beckwith, V. W. Bowry and K. U. Ingold, *J. Am. Chem. Soc.*, 1992, **114**, 4983.

23 M. Moller, H. Botti, C. Batthyany, H. Rubbo, R. Radi and A. Denicola, *J. Biol. Chem.*, 2005, **280**, 8850.

24 G. Merenyi, J. Lind and L. Engman, *J. Chem. Soc., Perkin Trans. 2*, 1994, 2551.

25 L. Eberson, *Electron Transfer Reactions in Organic Chemistry*, Springer-Verlag, Berlin, 1987.
26 L. R. C. Barclay, S. J. Locke, J. M. MacNeil, J. vanKessel, G. W. Burton and K. U. Ingold, *J. Am. Chem. Soc.*, 1984, **106**, 2479.
27 (*a*) P. Neta, R. E. Huie and A. B. Ross, *J. Phys. Chem. Ref. Data*, 1990, **19**, 413; (*b*) E. T. Denisov and T. G. Denisova, *Handbook of Antioxidants*, CRC Press, Boca Raton, Florida, 2000.
28 K. U. Ingold and D. A. Pratt, *Chem. Rev.*, 2014, **114**, 9022.
29 J. L. Hodgson and M. L. Coote, *Macromolecules*, 2010, **43**, 4573.
30 K. Krumova, S. Friedland and G. Cosa, *J. Am. Chem. Soc.*, 2012, **134**, 10102.
31 A. M. Samuni, A. Lipman and Y. Barenholz, *Chem. Phys. Lipids*, 2000, **105**, 121.
32 (*a*) P. Stipa, *Chem. Phys.*, 2006, **323**, 501; (*b*) P. Stipa, *Tetrahedron*, 2013, **69**, 4591; (*c*) F. Neese, *Wiley Interdiscip. Rev.: Comput. Mol. Sci.*, 2012, **2**, 73.
33 (*a*) A. Collauto, A. Barbon, M. Zerbetto and M. Brustolon, *Mol. Phys.*, 2013, **111**, 2933; (*b*) V. Barone, M. Brustolon, P. Cimino, A. Polimeno, M. Zerbetto and A. Zoleo, *J. Am. Chem. Soc.*, 2006, **128**, 15865.
34 E. G. Rozantsev, *Free Nitroxyl Radicals*, Plenum, 1970, p. 249.
35 (*a*) C. Bruno, R. Benassi, A. Passalacqua, F. Paolucci, C. Fontanesi, M. Marcaccio, E. A. Jackson and L. T. Scott, *J. Phys. Chem. B*, 2009, **113**, 1954; (*b*) A. A. La Pensee, J. Bickley, S. J. Higgins, M. Marcaccio, F. Paolucci, S. Roffia and J. M. Charnock, *J. Chem. Soc., Dalton Trans.*, 2002, 4095.
36 G. Angelini, M. Pisani, G. Mobbili, M. Marini and C. Gasbarri, *Biochim. Biophys. Acta, Biomembr.*, 2013, **1828**, 2506.
37 M. Marcaccio, F. Paolucci, C. Paradisi, M. Carano, S. Roffia, C. Fontanesi, L. J. Yellowlees, S. Serroni, S. Campagna and V. Balzani, *J. Electroanal. Chem.*, 2002, **532**, 99.
38 C. Amatore and C. Lefrou, *J. Electroanal. Chem.*, 1992, **324**, 33.
39 L. Mottier, in *Antigona*, University of Bologna, Bologna, Italy, 1999.
40 C. Altenbach, W. Froncisz, R. Hemker, H. McHaourab and W. L. Hubbell, *Biophys. J.*, 2005, **89**, 2103.
41 M. P. Nieh, C. J. Glinka, S. Krueger, R. S. Prosser and J. Katsaras, *Langmuir*, 2001, **17**, 2629.
42 (*a*) Z. C. Liang, Y. Lou, J. H. Freed, L. Columbus and W. L. Hubbell, *J. Phys. Chem. B*, 2004, **108**, 17649; (*b*) B. M. Kroncke, P. S. Horanyi and L. Columbus, *Biochemistry*, 2010, **49**, 10045; (*c*) D. J. Xu, R. H. Crepeau, C. K. Ober and J. H. Freed, *J. Phys. Chem.*, 1996, **100**, 15873; (*d*) L. Hoffman, R. A. Stein, R. J. Colbran and H. S. Mchaourab, *EMBO J.*, 2011, **30**, 1251; (*e*) J. P. Barnes, Z. C. Liang, H. S. Mchaourab, J. H. Freed and W. L. Hubbell, *Biophys. J.*, 1999, **76**, 3298.
43 D. Kurad, G. Jeschke and D. Marsh, *Appl. Magn. Reson.*, 2001, **21**, 469.
44 J. A. Buege and S. D. Aust, *Methods Enzymol.*, 1978, **52**, 302.